Temperature-dependent thermal properties of single-walled carbon nanotube thin films

A. Duzynska,[1] A. Taube,[1,a)] K. P. Korona,[2] J. Judek,[1] and M. Zdrojek[1,b)]
[1]*Faculty of Physics, Warsaw University of Technology, Koszykowa 75, Warsaw 00-662, Poland*
[2]*Faculty of Physics, University of Warsaw, Pasteura 5, Warsaw 02-093, Poland*

(Received 12 March 2015; accepted 24 April 2015; published online 6 May 2015)

We herein report the determination of the intrinsic thermal conductivity (κ) and interfacial thermal conductance (g) of single-walled carbon nanotube thin films (50 nm) on top of a SiO_2 substrate. The study was performed as a function of temperature (300–450 K) using the opto-thermal technique. The value of κ decreases nonlinearly by approximately 60% from a value of 26 Wm^{-1} K^{-1} at 300 K to a value of 9 Wm^{-1} K^{-1} at 450 K. This effect stems from the increase of multi-phonon scattering at higher temperatures. The g increases with temperature, reaching a saturation plateau at 410 K. These findings may contribute to a better understanding of the thermal properties of the supported carbon nanotube thin films, which are crucial for any heat dissipation applications. © *2015 AIP Publishing LLC*. [http://dx.doi.org/10.1063/1.4919792]

Carbon nanotubes (CNTs) have been intensively investigated during the last 20 years because of their exceptional electrical,[1] mechanical,[2] optical,[3] and thermal properties.[4] These particular properties stimulated exploratory research for a wide variety of applications, e.g., heat spreaders,[5] electrical interconnects,[6] solar cells,[7] and supercapacitors.[8] For instance, by harnessing the high thermal and electrical conductivity of CNTs,[9] a potential candidate for next-generation interconnects materials may be produced.[6] For the design of this application (and many others), knowledge of the thermal properties of carbon nanotubes, such as thermal conductivity (κ) and interfacial thermal conductance (g), is of great importance.

Many previous works have addressed the issue of determination of the thermal properties of individual CNT structures using different methods, e.g., opto-thermal,[10] thermal bridge,[11] or 3ω.[12] Therefore, it is known that the room temperature thermal conductivity of individual single wall CNTs (SWCNTs) may be very high, exceeding 3000 Wm^{-1} K^{-1}.[13] However, for practical applications, more complex carbon nanotube structures are needed such as CNT bundles or especially thin CNT films. However, the complexity of the structure and various synthetic methods of such carbon systems introduce wide divergence in the thermal conductivity values,[14] often leading to a significant decrease in the values to as low as 0.1 Wm^{-1} K^{-1} for random networks[15] or 2.3 Wm^{-1} K^{-1} for carbon nanotube mats.[11] Other studies have shown a value of 18.3 Wm^{-1} K^{-1} (Ref. 16) for suspended high-density SWCNT thin films and values from 8 to 20 Wm^{-1} K^{-1} (Ref. 17) for different multiwall carbon nanotube (MWCNT) mats. Determination of the room temperature thermal conductivity of thin CNT films from tubes produced by different methods has been demonstrated,[14] showing no dependence of κ on the thickness of the film. Relatively thick (several μm) un-aligned nanotube ropes were used to measure the temperature dependence of thermal conductivity below 300 K, showing a decrease of κ with decreasing temperature.[18]

Temperature-dependence of various CNT mats/bundles has been reported in the literature. For example, Sinha *et al.*[19] reported $\kappa(T)$ dependency for as-grown (CVD) and sparse MWCNT and SWCNT-films, showing an remarkably slight (linear) increase of κ from approximately 1.5 Wm^{-1} K^{-1} at 300 K by ~8% at 380 K. Aliev *et al.*[20] studied the thermal conductivity of differently aligned MWCNTs (forest, bundles, and sheets) in the temperature range of (70–320) K demonstrating significant change upon temperature and length of the samples, from κ ~15 Wm^{-1} K^{-1} at 70 K up to several hundred Wm^{-1} K^{-1} at room temperature. More studies can be read in the recent review by Marconnet *et al.*[9]

The interfacial contact conductance also plays an important role in the thermal properties of thin films laying on substrates.[9] For instance, the value of this quantity was theoretically estimated to be ~5.8×10^7 W/m^2K for various diameters of separated SWCNTs on a SiO_2 substrate, and this value was dependent on temperature.[21] Other reports have demonstrated the CNT-substrate thermal boundary resistance for vertically aligned carbon nanotube arrays and different substrates, e.g., SiO_2,[22] or SiC.[23] However, until now, there are no studies of the interfacial contact conductance between horizontally aligned CNT thin films and the substrate.

In this work, we measure the intrinsic temperature-dependent thermal conductivity and interfacial thermal conductance of a high-density semiconducting single-walled carbon nanotube thin film on a SiO_2/Si substrate. We show that the thermal properties (κ and g) of the SWCNT film change significantly as a function of temperature in the range of 300–450 K. These findings may contribute to a better understanding of the thermal properties of supported CNT thin films, which are crucial for any heat dissipation applications.

To assess the thermal properties of thin CNT films, we utilized a Raman spectroscopy technique and an approach

[a)]Also at the Institute of Electron Technology, Warsaw, Poland and the Institute of Microelectronics and Optoelectronics, Warsaw University of Technology, Warsaw, Poland.
[b)]Author to whom correspondence should be addressed. Electronic mail: zdrojek@if.pw.edu.pl

developed by Balandin *et al.*[24] for graphene and later adopted and extended by Ghosh *et al.*,[25] Chen *et al.*,[26] and Cai *et al.*[27] (See also, a comprehensive review on thermal properties of carbon materials—Balandin.[28]) We chose the Raman technique because it is a simple and reliable method for the characterization of thermal properties of nanomaterials. Thus far, this method has been applied to study the thermal properties of CNTs (individual and films),[10,29] graphene,[27] WS_2,[30] and MoS_2.[31,32] The mentioned approach enables calculation of the thermal conductivity (κ) and the interfacial thermal conductance per unit area (g) using the local temperatures (depending on the heat transport ability of the material) provided by Raman studies with different heating powers. Importantly, this approach enables derivation of the intrinsic (volumetric) film thermal conductivity because it does not require any contacts to the measured film.

CNT thin films were fabricated using well-dispersed water solutions of semiconducting SWCNTs from NanoIntegris (Iso-Nanotubes-S, 99% purity). Initially, the nanotubes were stabilized by a combination of ionic surfactants. The tube diameters were in the range of 1.2–1.7 nm with a mean length of 1 μm and a concentration in solution of 0.01 mg/ml. The thin films were prepared by a standard vacuum filtration process.[33] A specified amount of carbon nanotube solution was filtered onto the mixed cellulose ester membrane (Millipore, 0.025 μm pore-size, 25 mm diameter) to obtain the desired thickness of the film. Residual surfactant in the film/filter "sandwich" was rinsed away with deionized water. After the filtration process in the first step, the membrane with the SWCNTs film was dried and then left in toluene for a few hours. Next, a 5 × 5 mm section of the SWCNT film-coated membrane was cut and transferred face down onto a SiO_2/Si substrate (1 μm thickness of silicon dioxide). A cellulose membrane was dissolved in the vapors of acetone. Then, a sample was immersed into liquid acetone to remove any residual filter. Finally, the sample was rinsed with methanol and gently dried with nitrogen. Notably, no crosslinking solution or residual surfactant was observed between the carbon nanotubes in the final film structure (confirmed by Raman measurements).

Atomic force microscopy (AFM) and scanning electron microscopy (SEM) were employed to initially characterize the thin films. Fig. 1(a) shows an SEM image of the SWCNT film. The film thickness, determined by the AFM measurements, was approximately 50 nm. The absorbance spectra of our films (fabricated on the glass substrate) were collected using a Cary 5000 spectrometer (see Fig. 3(d) for details).

The temperature-dependent Raman spectra were collected using a Renishaw spectrometer with a 514 nm Ar laser excitation line. A schematic of the experimental setup is shown in Fig. 1(b). The carbon nanotube thin film on the SiO_2/Si substrate was illuminated by the laser beam from the Raman spectrometer. In the experiment, we used two objectives with magnifications of 20× and 100×, with different numerical apertures (NA = 0.4 and 0.85, respectively), and in a consequently different laser beam radius. In this configuration, the laser beam is not only a source of photons which scatter during Raman measurements but also a heat factor (use of higher laser power can increase the local temperature of the sample). To measure the temperature-dependent Raman spectra, a sample was placed on the hot plate, which enabled change of the temperature from 300 to 450 K with a stability of 0.1 K at ambient conditions. To determine the local temperature of the SWCNT film upon laser heating, we used the Raman G^+ line position because its intensity is higher than the G^- mode and enables more precise determination of the Raman mode position.[29]

Fig. 2(a) presents the normalized Raman spectra of the SWCNT thin film at selected temperatures from 300 to 450 K measured using the 20× objective and 0.16 mW incident laser power (where laser heating is not expected). Detailed data obtained from temperature-dependent Raman measurements of the G^+ peak for different objectives and incident laser powers are presented in Fig. 2(b).

To describe the temperature dependence of the G^+ peak position, we used a linear fit with formula[34]

$$\omega(T) = \omega_0 + \chi T, \tag{1}$$

where ω_0 is the phonon frequency at zero temperature and χ is the first-order temperature coefficient. The fitted χ parameters are presented in Fig. 2(b) for each data series. Measurements were performed for an objective with magnification 20× (incident laser powers (P_L) of 0.16 mW and 1.33 mW) and 100× (incident laser powers of 0.04 mW and 0.31 mW). These data are further used for calculation of the film thermal properties (adopting the model of Cai *et al.*[27]).

We performed measurements for two power levels; however, we performed several measurements for each power level at each global temperature to obtain more reliable and more accurate results. We used such power levels to effectively heat the film and obtain substantial Raman shift of the G^+ mode position while not damaging it at the same time. The laser power range was carefully tested before using on the samples.

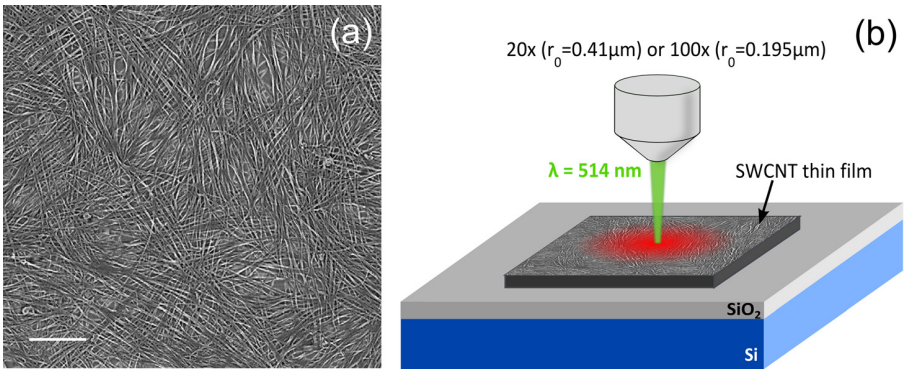

FIG. 1. (a) SEM image of a high-density SWCNT thin film, the scale bar represents 400 nm. (b) Schematic of the Raman experimental setup (SWCNT film thickness 50 nm), which is the beam radius for different objectives.

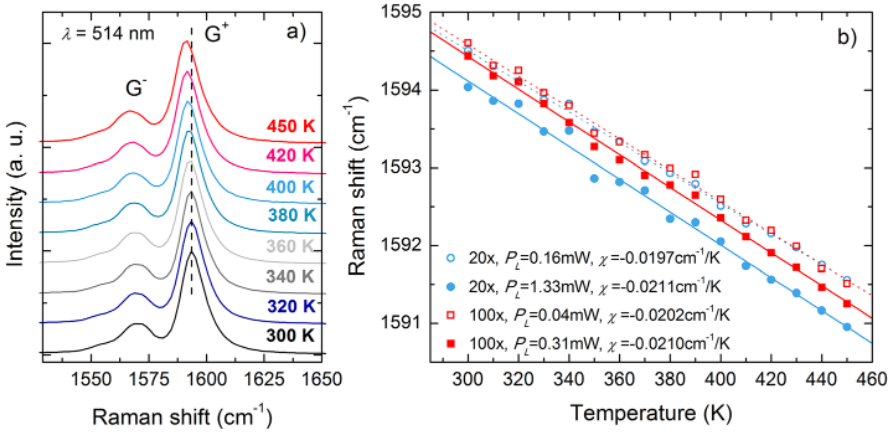

FIG. 2. (a) An example of normalized Raman spectra for the SWCNT thin film measured at selected temperatures ranging from 300 to 450 K with a 20× objective and 0.16 mW incident laser power. (b) Temperature dependence of the Raman G^+ peak position for a SWCNT thin film measured for two objectives, 20× and 100×, and different incident laser powers. The lines represent a fit to Eq. (1). The average uncertainty of the determination of a peak position was $<0.2\,\mathrm{cm}^{-1}$ (error bars not shown for clarity).

The different results for the two objectives come from the different laser beam sizes (r_0) for objectives with different NA. The 100× objective had a smaller beam size, thus, the heat power density was higher than in the case of the 50× objective (for the same laser power level). As a consequence, the temperature rise generated by the heat source with smaller r_0 and the temperature measured by Raman spectroscopy is higher. This result corresponds to larger Raman shifts, as depicted in Fig. 2(b).

As the starting point for determining the thermal properties (κ and g) of CNT films is the heat diffusion equation in cylindrical coordination

$$\frac{1}{r}\frac{d}{dr}\left(r\frac{dT}{dr}\right)-\frac{g}{\kappa t}(T-T_a)+\frac{Q}{\kappa}=0, \tag{2}$$

where κ is the thermal conductivity, g is the interfacial thermal conductance per unit area, t is the thickness of the CNT film (50 nm, obtained from AFM measurements), and T_a is the ambient temperature. In the performed experiment, volumetric optical heating is described by the above equation, assuming a Gaussian-type profile of the laser beam

$$Q=\frac{q_0}{t}e^{\left(\frac{-r^2}{r_0^2}\right)}, \tag{3}$$

where q_0 is the peak of absorbed laser power per unit area at the center of the beam spot and r_0 is the beam radius. The r_0 was calculated using the formula $r_0=\lambda/\pi NA$ (where NA is the numerical aperture of each lens), and was determined to be 0.41 μm and 0.195 μm for 20× and 100× lenses, respectively. Then, the temperature rise as a result of optical heating, $\theta\equiv(T\text{-}T_a)$, was introduced. Using the solution of Eq. (2), the temperature rise measured in the Raman spectra can be expressed by

$$\theta_m=\frac{\int_0^\infty \theta(r)e^{\left(\frac{-r^2}{r_0^2}\right)}rdr}{\int_0^\infty e^{\left(\frac{-r^2}{r_0^2}\right)}rdr}. \tag{4}$$

Furthermore, we used a quantity, defined as $\frac{\partial\theta_m}{\partial P_{abs}}$ (where P_{abs} is absorbed laser power), that can be experimentally obtained from the following equation:

$$\frac{\partial\theta_m}{\partial P_{abs}}=\frac{\partial\omega}{\partial P_{abs}}\frac{\partial T}{\partial\omega}=\frac{\partial\omega}{\partial P_{abs}}\chi^{-1}, \tag{5}$$

where χ is the temperature coefficient derived earlier from the measured temperature-dependent Raman spectra. Using $(\partial\theta_m/\partial P_{abs})$ instead of the measured temperature rise (θ_m) allows us to avoid calibration errors from the optical systems for both lenses used in the experiment.

The thermal properties were then derived by the solution of the system of Eq. (5) for two different lenses with different beam radii because the solution of Eq. (2) depends only on two unknown parameters, κ and g.

The $(\partial\theta_m/\partial P_{abs})$ is determined from experimental data in the following manner. First, for each global temperature, $(\partial\omega/\partial P_{abs})$ is calculated from the position of the G^+ mode dependence on the absorbed laser power. The absorbed laser power (P_{abs}) was calculated as the incident laser power times the absorbance level. The absorbance spectrum of the CNT film on the glass substrate used in this experiment was measured and is depicted in Fig. 3(d). For the excitation wavelength utilized herein ($\lambda=514$ nm), the absorbance level (α) was approximately 11% (noted by an arrow on Fig. 3(d)).

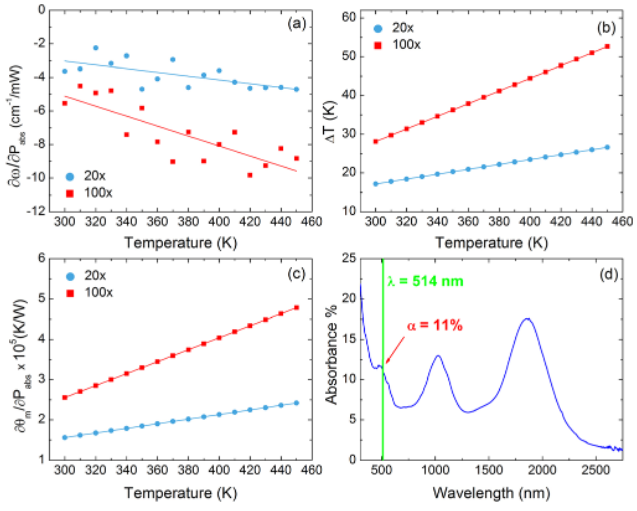

FIG. 3. Calculated (a) $(\partial\omega/\partial P_{abs})$, (b) $\Delta T=T\text{-}T_a$, and (c) $(\partial\theta_m/\partial P_{abs})$ values as a function of global temperature for the 20× and 100× objectives for a SWCNT thin film. (d) Absorbance spectra of the SWCNT thin film on glass.

We note that measured value of α indicates that the laser light penetrates entire film through. This is also evidenced by the presence of the Si peak ($\sim$520 cm^{-1}) in the Raman spectra (data not shown here). Thus, the heat dissipates radially from the center not only on the surface of the film but also within.

The $(\partial\omega/\partial P_{abs})$ was calculated for two lenses as the difference between the G^+ mode position for two P_{abs} levels, which was linearly fitted. Then, by extrapolation of the fitted data to $P_{abs} = 0$, the temperature dependence of the G^+ mode position was calculated, and the χ parameter was obtained for each lens. Finally, the experimental value of $(\partial\theta_m/\partial P_{abs})$ was obtained on the basis of Eq. (5).

To determine the thermal properties of the CNT film, these values were interposed to the systems of Eq. (5), which was solved for each global temperature. The calculated temperature dependence of the values $(\partial\omega/\partial P_{abs})$, $\Delta T = T - T_a$, and $(\partial\theta_m/\partial P_{abs})$, for both lenses are presented in Fig. 3. It can be clearly observed that the values of ΔT for the 20× and 100× objectives are different, which is associated with the various laser power densities and r_0 values for each lens. The obtained slopes of the $(\partial\theta_m/\partial P_{abs})$ values were 573 and 1487 K/W for the 20× and 100× objectives, respectively.

In the next step, the calculated thermal conductivity and interfacial thermal conductance of the SWCNT film were determined for the $(\partial\theta_m/\partial P_{abs})$ value at each measured temperature, which are shown in Fig. 4. First, at room temperature, the value of κ was found to be approximately 26 W/mK and is within the relatively large range from 0.13 W/mK to over 250 W/mK reported in the literature (see Ref. 9). The main factors responsible for the significant discrepancy in the determination of thermal conductivity are the tube-tube junctions, the alignment, the filling factor of the system,[9] and the substrate, as well as the different measurement methods[9,35] and environments. We note here that our measurements of the thermal properties took place under ambient conditions and not in vacuum as in many cases. This approach is important because it represents the most applicable configuration.

The thermal conductivity was found to exhibit a nonlinear temperature dependence, decreasing with temperature from 26.4 Wm^{-1} K^{-1} at room temperature to 9.2 Wm^{-1} K^{-1} at 450 K, showing a nearly 60% drop. This trend appears to be consistent with the Umklapp phonon-phonon scattering process, in which both first and second order contributions (Ref. 36) lead to a $\kappa(T)$ that scales as $(aT + bT^2)^{-1}$, where a and b are constants. The fit obtained from the temperature-dependent data is shown in Fig. 4. Interestingly, a very similar trend was observed in the case of an individual SWCNT above room temperature by Pop *et al.*,[36] demonstrating that the nature of the heat dissipation processes in individual tubes are similar to those in more complex systems such as densely packed CNT films. Another possible explanation is that in 50 nm thick and dense film, the boundary phonon scattering (at the tube-tube interface) may be much stronger than the second-order phonon-phonon scattering. However, there is a lack in the literature on this issue, but theoretical estimation for graphene shows that the second-order processes limits the thermal conductivity in graphene nanoribons with average size above 100 μm.[37]

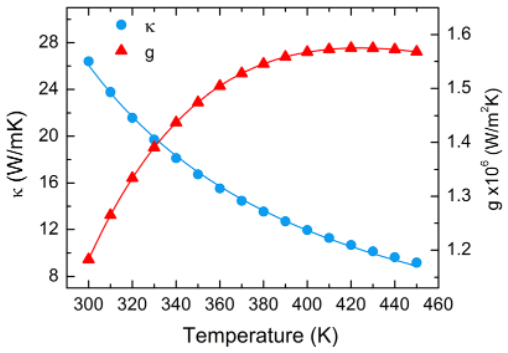

FIG. 4. Point stats for calculated values of κ and g as a function of global temperature. The blue curve represents fit to the data using the function $(aT + bT^2)^{-1}$, where $a = -(117 \pm 4) \times 10^{-6}$ m/W and $b = (82 \pm 1) \times 10^{-8}$ m/WK. The g curve (red) is only a guide for the eye.

The interfacial thermal conductance exhibits nonlinear characteristics, increasing from 1.18 to 1.57 MWm^{-2} K^{-1} in the temperature range of 300–450 K, reaching a saturation plateau at approximately 410 K. The value of g needs to be considered with care because it is directly proportional to the substrate-CNT film interaction strength (see Ref. 21 and the references within). By contrast, the linear dependence of $g(T)$ in the case of individual tubes reported by Ong and Pop[21] were observed to strongly increase nonlinearly with g to a saturation plateau at 410 K. However, this trend is similar to that observed for a multilayer graphene system on a SiO_2 substrate.[38]

We note that the value of the interfacial thermal conductance at the interface between the thin film and the substrate may influence the value of κ. Our calculations show that a 10% change of g will change κ by nearly 7% at 300 K and 12% at 450 K.

In conclusion, we herein report the thermal conductivity of supported semiconducting SWCNT thin films as a function of temperature under ambient conditions, designated by the Raman method. We found that the thermal conductivity has nonlinear characteristics and decreases from 26.4 to 9.2 Wm^{-1} K^{-1} in the temperature range of 300–450 K. A decrease of the thermal conductivity is associated with the increase of higher order phonon scattering processes. We show that that the value of g increases with temperature, reaching a saturation plateau at 410 K. These findings may contribute to a better understanding of the thermal properties of supported CNT thin films, which are crucial for any heat dissipation application.

This work was supported by the Preludium project funded by NCN (2014/13/N/ST5/01255). A.T. was supported by the Polish Ministry of Science within the Diamond Grant Program (0025/DIA/2013/42). M.Z. acknowledges support for the project (Lider/11/22/L-2/10/NCBR/2011).

The authors declare no competing financial interest.

[1]J. Sandler, M. S. Shaffer, T. Prasse, W. Bauhofer, K. Schulte, and A. H. Windle, Polymer **40**, 5967 (1999).
[2]G. Overney, W. Zhoung, and D. Tománek, Z. Phys. D: At. Mol. Clusters **27**, 93 (1993).

[3]H. Kataura, Y. Kumazawa, Y. Maniwa, I. Umezu, S. Suzuki, Y. Ohtsuka, and Y. Achiba, Synth. Met. **103**, 2555 (1999).
[4]J. Che, T. Çağin, and W. A. Goddard III, Nanotechnology **11**, 65 (2000).
[5]K. H. Baloch, N. Voskanian, and J. Cumings, Appl. Phys. Lett. **97**, 063105 (2010).
[6]F. Kreupl, A. P. Graham, G. S. Duesberg, W. Steinhögl, M. Liebau, E. Unger, and W. Hönlein, Microelectron. Eng. **64**, 399 (2002).
[7]M. W. Rowell, M. A. Topinka, M. D. McGehee, H. Prall, G. Dennler, N. S. Sariciftci, L. Hu, and G. Gruner, Appl. Phys. Lett. **88**, 233506 (2006).
[8]E. Frackowiak, K. Metenier, V. Bertagna, and F. Beguin, Appl. Phys. Lett. **77**, 2421 (2000).
[9]A. M. Marconnet, M. A. Panzer, and K. E. Goodson, Rev. Mod. Phys. **85**, 1295 (2013).
[10]Q. Li, C. Liu, X. Wang, and S. Fan, Nanotechnology **20**, 145702 (2009).
[11]J. Hone, M. Whitney, C. Piskoti, and A. Zettl, Phys. Rev. B **59**, R2514 (1999).
[12]J. Hou, X. Wang, P. Vellelacheruvu, and J. Guo, J. Appl. Phys. **100**, 124314 (2006).
[13]C. Yu, L. Shi, Z. Yao, D. Li, and A. Majumdar, Nano Lett. **5**, 1842 (2005).
[14]D. Kim, L. Zhu, C. Han, J. Kim, and S. Baik, Langmuir **27**, 14532 (2011).
[15]R. S. Prasher, X. J. Hu, Y. Chalopin, N. Mingo, K. Lofgreen, S. Volz, F. Cleri, and P. Keblinski, Phys. Rev. Lett. **102**, 105901 (2009).
[16]S. Sahoo, V. R. Chitturi, R. Agarwal, J. Jiang, and R. S. Katiyar, ACS Appl. Mater. Interfaces **6**, 19958 (2014).
[17]Y. J. Heo, C. H. Yun, W. N. Kim, and H. S. Lee, Curr. Appl. Phys. **11**, 1144 (2011).
[18]J. Hone, M. C. Llaguno, N. M. Nemes, A. T. Johnson, J. E. Fischer, D. A. Walters, M. J. Casavant, J. Schmidt, and R. E. Smalley, Appl. Phys. Lett. **77**, 666 (2000).
[19]S. Sinha, S. Barjami, G. Iannacchione, A. Schwab, and G. Muench, J. Nanopart. Res. **7**, 651 (2005).
[20]A. E. Aliev, M. H. Lima, E. M. Silverman, and R. H. Baughman, Nanotechnology **21**, 035709 (2010).
[21]Z. Ong and E. Pop, Phys. Rev. B **81**, 155408 (2010).
[22]Y. Son, S. K. Pal, T. Borca-Tasciuc, P. M. Ajayan, and R. W. Siegel, J. Appl. Phys. **103**, 024911 (2008).
[23]B. A. Cola, X. Xu, T. S. Fisher, M. A. Capano, and P. B. Amama, Nanoscale Microscale Thermophys. Eng. **12**, 228 (2008).
[24]A. A. Balandin, S. Ghosh, W. Bao, I. Calizo, D. Teweldebrhan, F. Miao, and C. N. Lau, Nano Lett. **8**, 902 (2008).
[25]S. Ghosh, W. Bao, D. L. Nika, S. Subrina, E. P. Pokatilov, C. N. Lau, and A. A. Balandin, Nat. Mater. **7**, 555 (2010).
[26]S. Chen, Q. Wu, C. Mishra, J. Kang, H. Zhang, K. Cho, W. Cai, A. A. Balandin, and R. S. Ruoff, Nat. Mater. **11**, 203 (2012).
[27]W. Cai, A. L. Moore, Y. Zhu, X. Li, S. Chen, L. Shi, and R. S. Ruoff, Nano Lett. **10**, 1645 (2010).
[28]A. A. Balandin, Nat. Mater. **10**, 569 (2011).
[29]A. Duzynska, J. Judek, and M. Zdrojek, Appl. Phys. Lett. **105**, 213105 (2014).
[30]M. Thripuranthaka and L. J. Dattatray, ACS Appl. Mater. Interfaces **6**, 1158 (2014).
[31]A. Taube, J. Judek, C. Jastrzębski, A. Duzynska, K. Świtkowski, and M. Zdrojek, ACS. Appl. Mater. Interfaces **6**, 8959 (2014).
[32]A. Taube, J. Judek, A. Łapińska, and M. Zdrojek, ACS Appl. Mater. Interfaces **7**, 5061 (2015).
[33]Z. Wu, Z. Chen, X. Du, J. M. Logan, J. Sippel, M. Nikolou, K. Kamaras, J. R. Reynolds, D. B. Tanner, A. F. Hebard, and A. G. Rinzler, Science **27**, 1273 (2004).
[34]I. Calizo, A. A. Balandin, W. Bao, F. Miao, and C. N. Lau, Nano Lett. **7**, 2645 (2007).
[35]L. Shi, D. Li, C. Yu, W. Jang, D. Kim, Z. Yao, P. Kim, and A. Majumdar, Heat Transfer **125**, 881 (2003).
[36]E. Pop, D. Mann, Q. Wang, K. Goodson, and H. Dai, Nano Lett. **6**, 96 (2006).
[37]D. L. Nika, A. S. Askerov, and A. A. Balandin, Nano Lett. **12**, 3238 (2012).
[38]Y. K. Koh, M. Bae, D. G. Cahill, and E. Pop, Nano Lett. **10**, 4363 (2010).